Supporting Information

Tailoring selenium dopant configurations for pH-universal CO_2 electroreduction to formate with ampere-level current density

Qizhou Xue,[#] [a] Jiaqi Feng,[#] *[a] Boyang Liu[a], Yanlin Wang[a], Aofei Cheng[a], Chongyang Jiang[b], Xiaofu Sun[c], Min Wang[b], Yinge Bai[b,d], Shaojuan Zeng,* [b,d] and Xiangping Zhang* [a,b]

1. State Key Laboratory of Heavy Oil Processing, College of Chemical Engineering and Environment, China University of Petroleum (Beijing), Beijing 102249, China

2. Beijing Key Laboratory of Ionic Liquids Clean Process, State Key Laboratory of Multiphase Complex Systems, CAS Key Laboratory of Green Process and Engineering, Institute of Process Engineering, Chinese Academy of Sciences, Beijing, 100190, China

3. Beijing National Laboratory for Molecular Sciences, Key Laboratory of Colloid and Interface and Thermodynamics, Center for Carbon Neutral Chemistry, Institute of Chemistry, Chinese Academy of Sciences, Beijing 100190, China

4. Huizhou Institute of Green Energy and Advanced Materials, Huizhou, Guangdong, 516081, China

* To whom correspondence should be addressed. Email: xpzhang@ipe.ac.cn
[#] These authors contributed equally to this article.

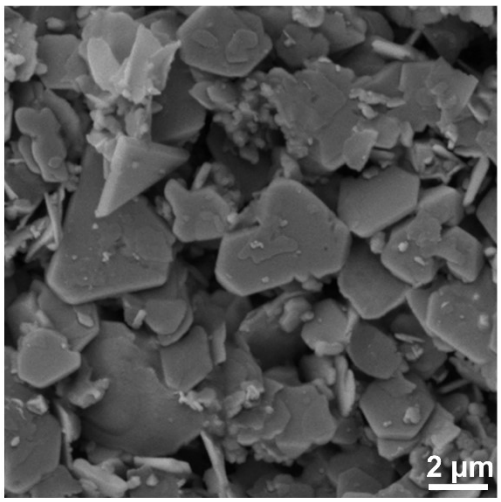

Figure S1. SEM image of Bi_2Se_3.

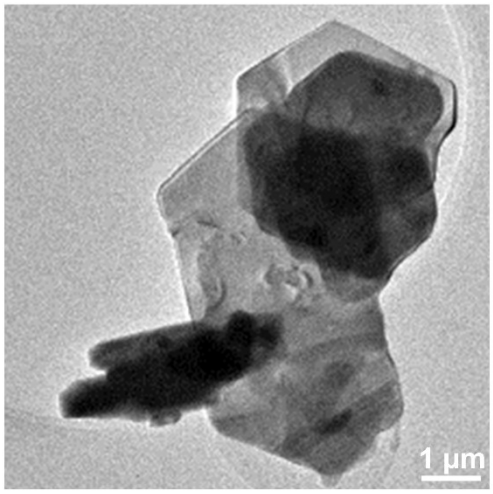

Figure S2. TEM image of Bi_2Se_3.

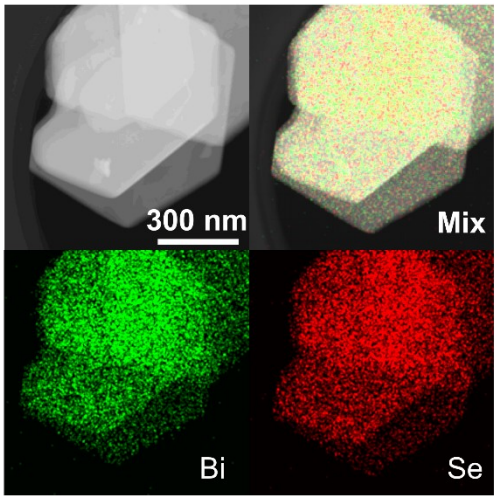

Figure S3. The EDS elemental mappings of Bi_2Se_3.

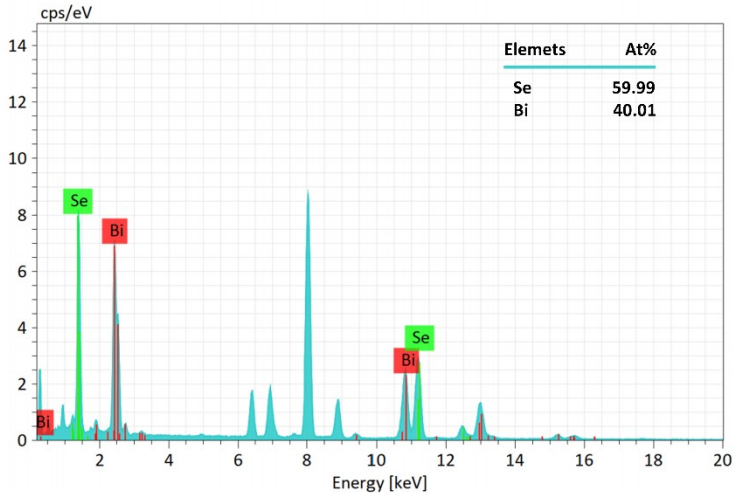

Figure S4. TEM-EDS spectrum of Bi_2Se_3.

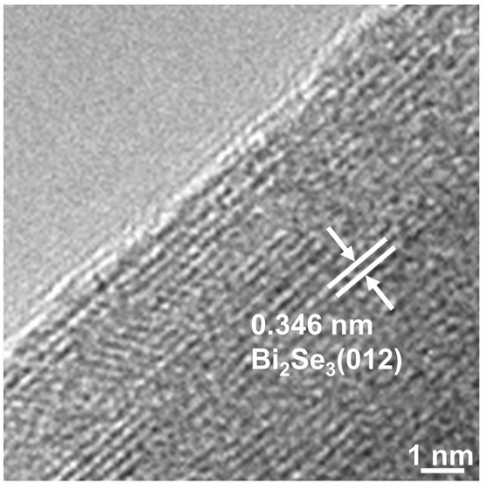

Figure S5. HRTEM image of Bi_2Se_3.

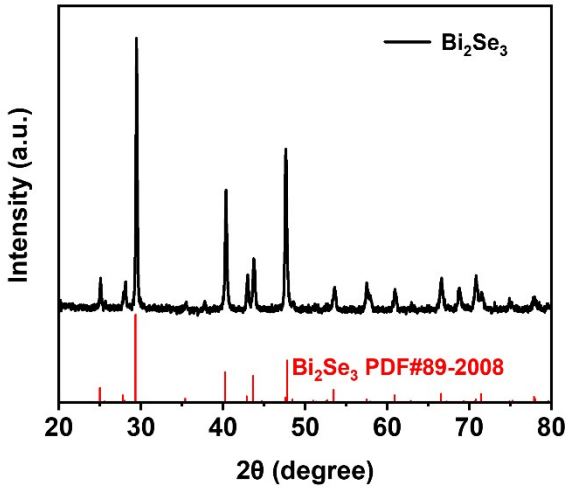

Figure S6. XRD pattern of Bi_2Se_3.

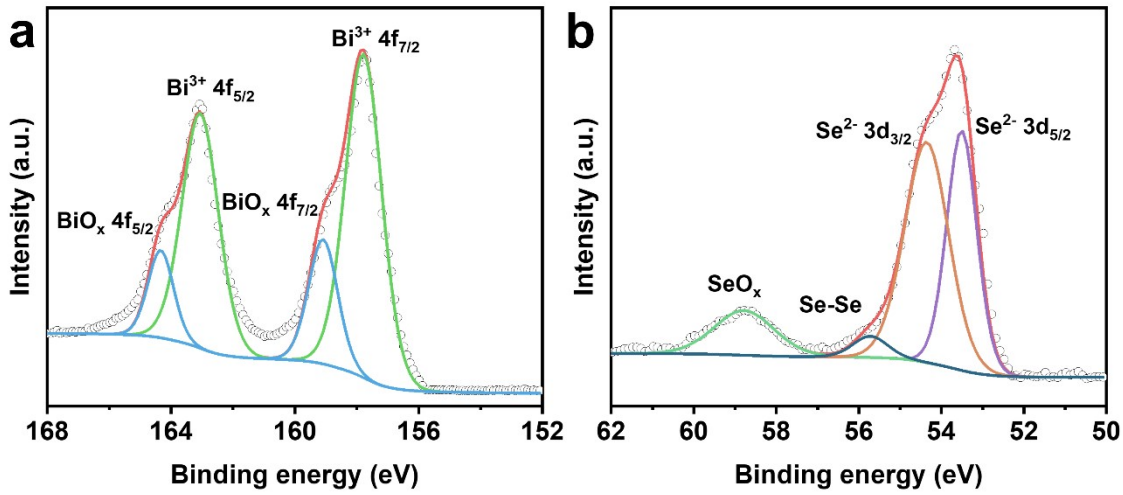

Figure S7. (a) Bi 4f and (b)Se 3d XPS spectra of Bi_2Se_3.

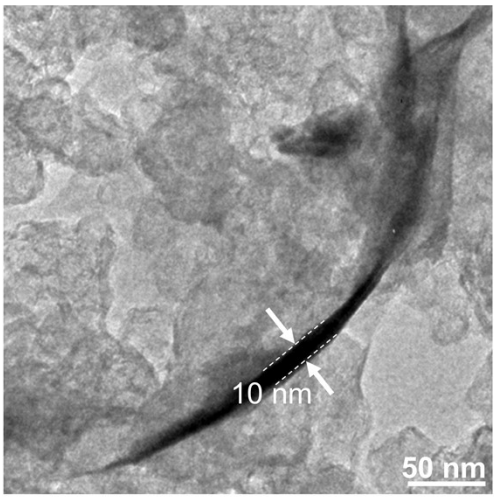

Figure S8. HRTEM image of Bi/Se-Inter.

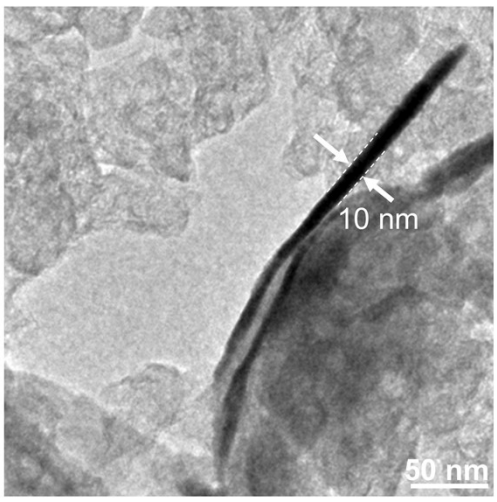

Figure S9. HRTEM image of Bi/Se-Subs.

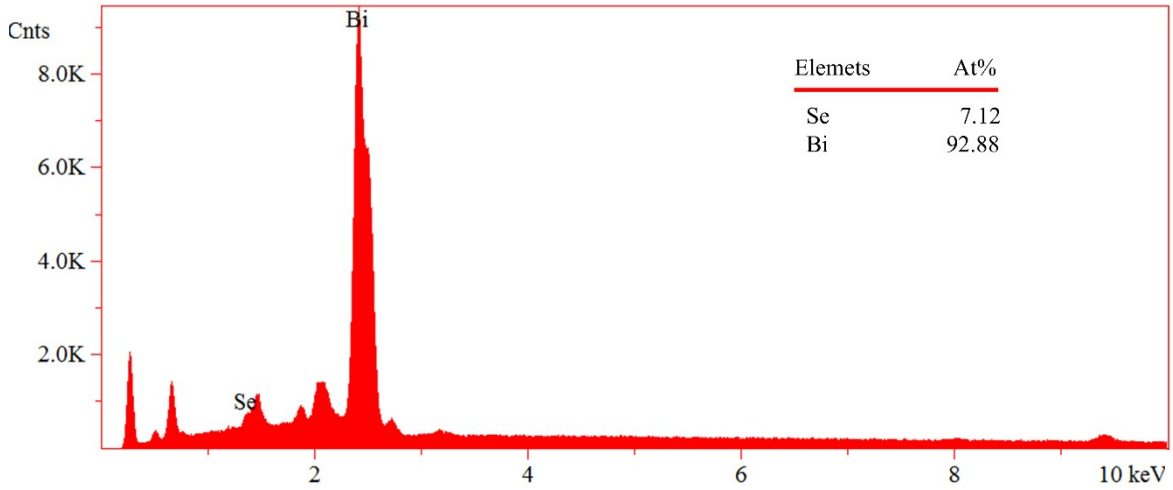

Figure S10. SEM-EDS spectrum of Bi/Se-Inter.

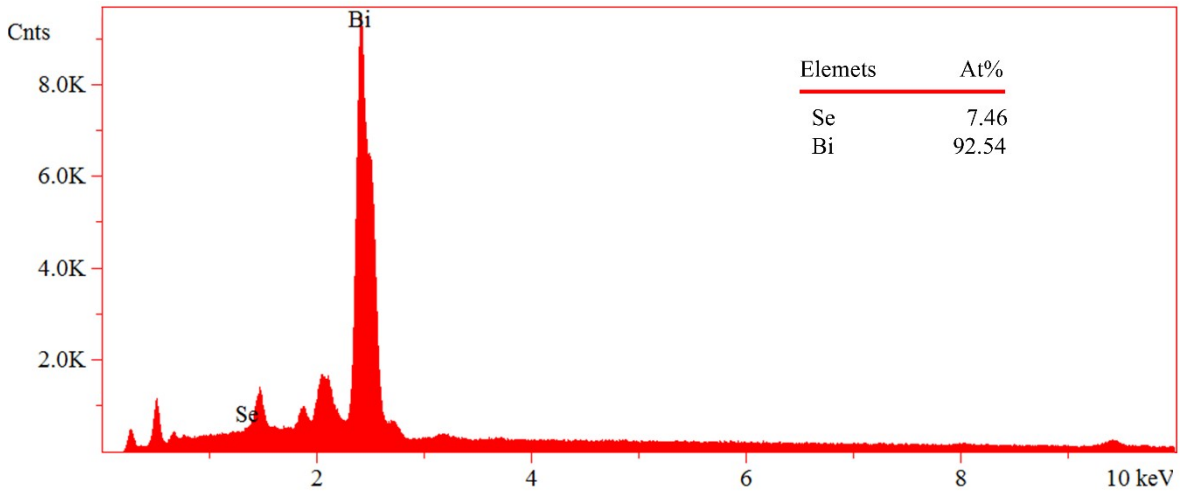

Figure S11. SEM-EDS spectrum of Bi/Se-Subs.

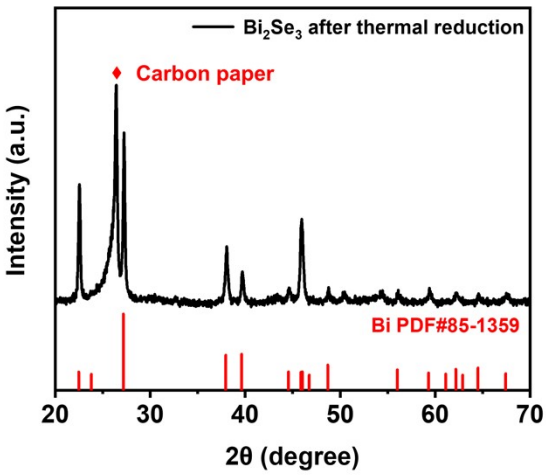

Figure S12. XRD pattern of Bi_2Se_3 after thermal reduction.

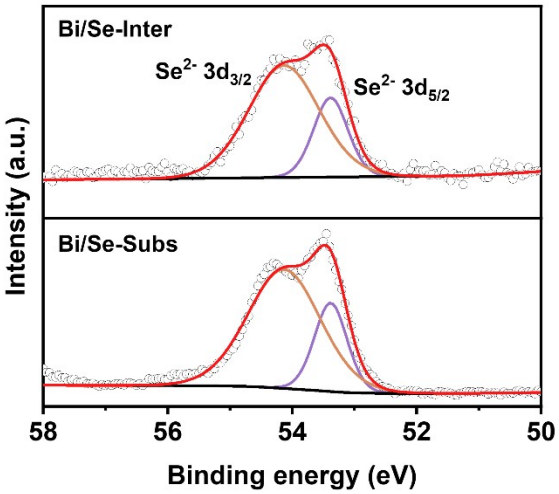

Figure S13. Se 3d XPS spectra of Bi/Se-Inter and Bi/Se-Subs.

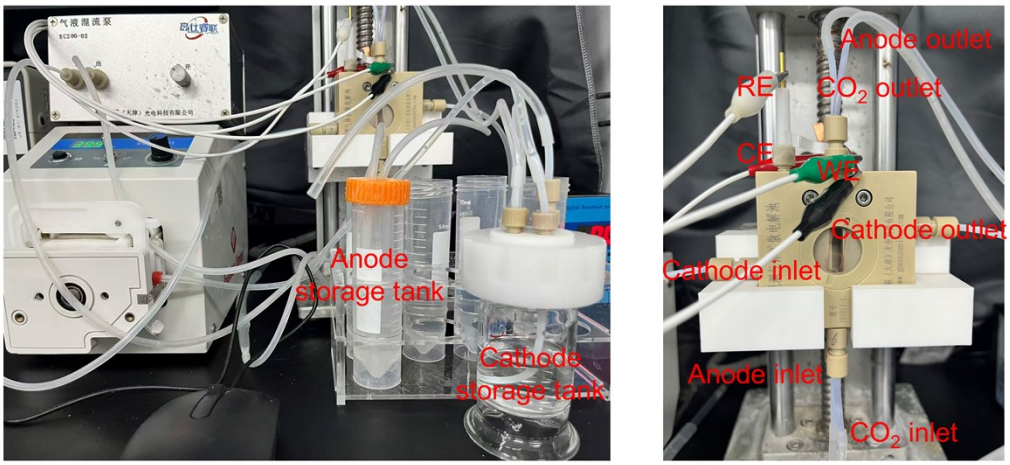

Figure S14. Digital photograph of the flow cell system.

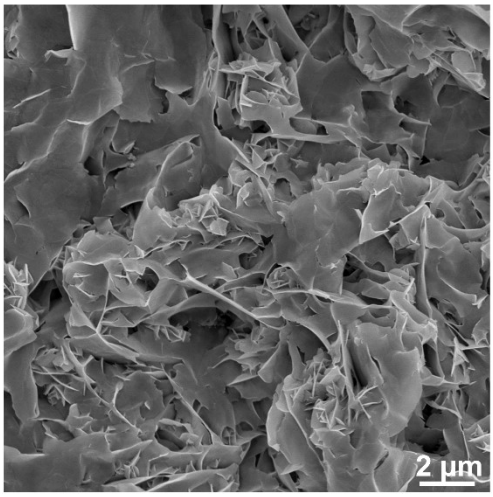

Figure S15. SEM image of Bi.

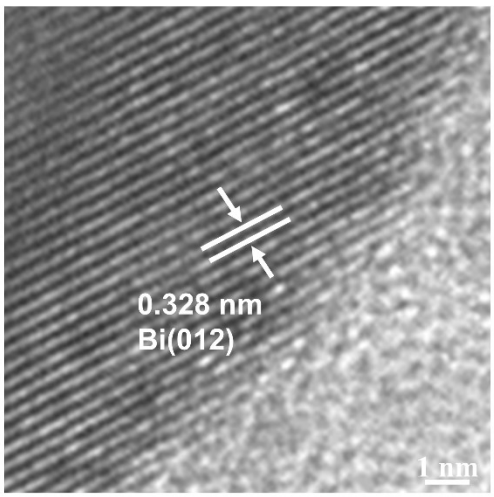

Figure S16. TEM image of Bi.

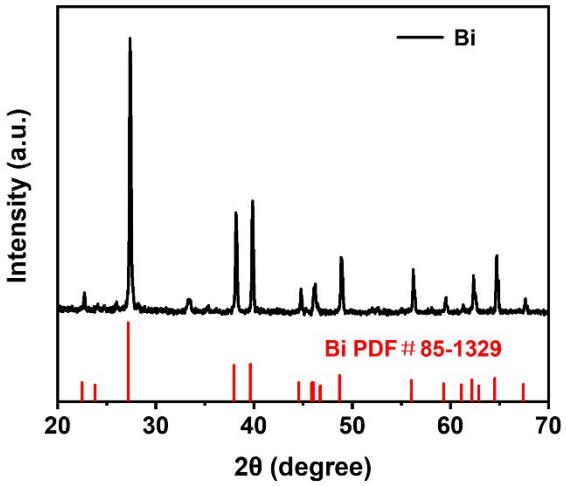

Figure S17. XRD pattern of Bi.

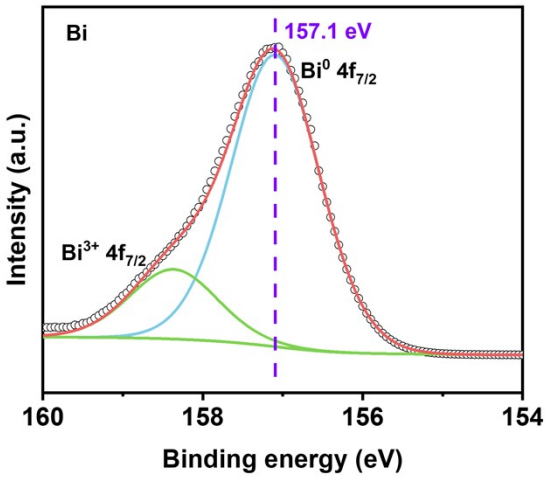

Figure S18. Bi 4f XPS spectrum of Bi.

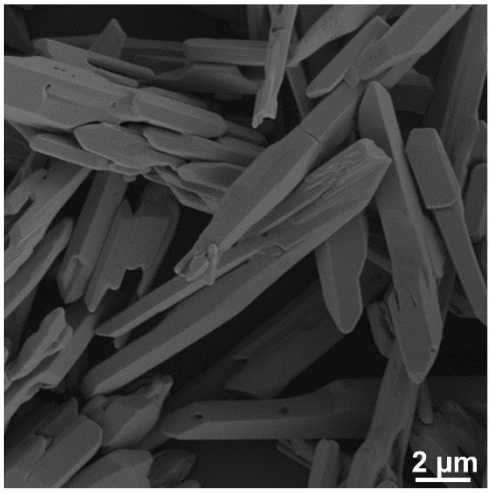

Figure S19. SEM image of Bi_2O_3.

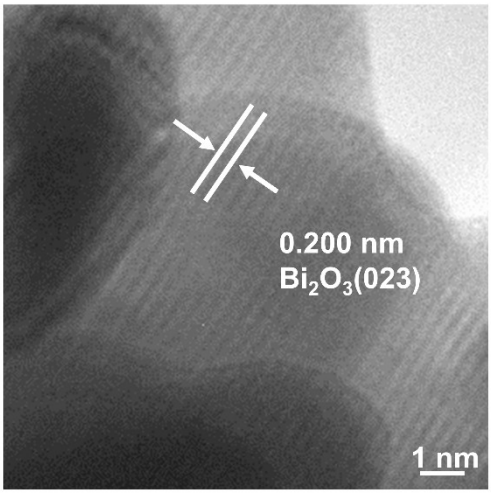

Figure S20. HRTME image of Bi_2O_3.

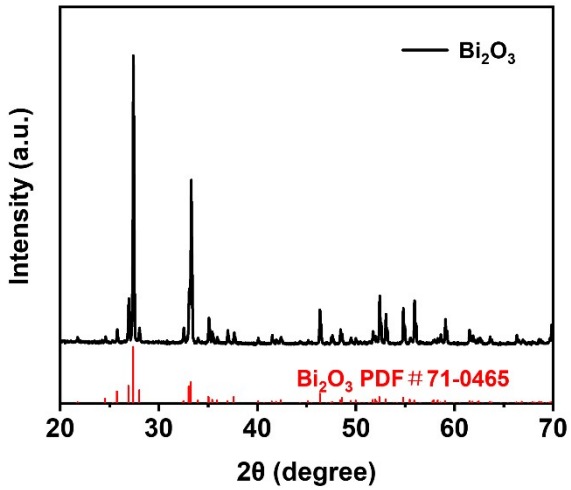

Figure S21. XRD pattern of Bi_2O_3.

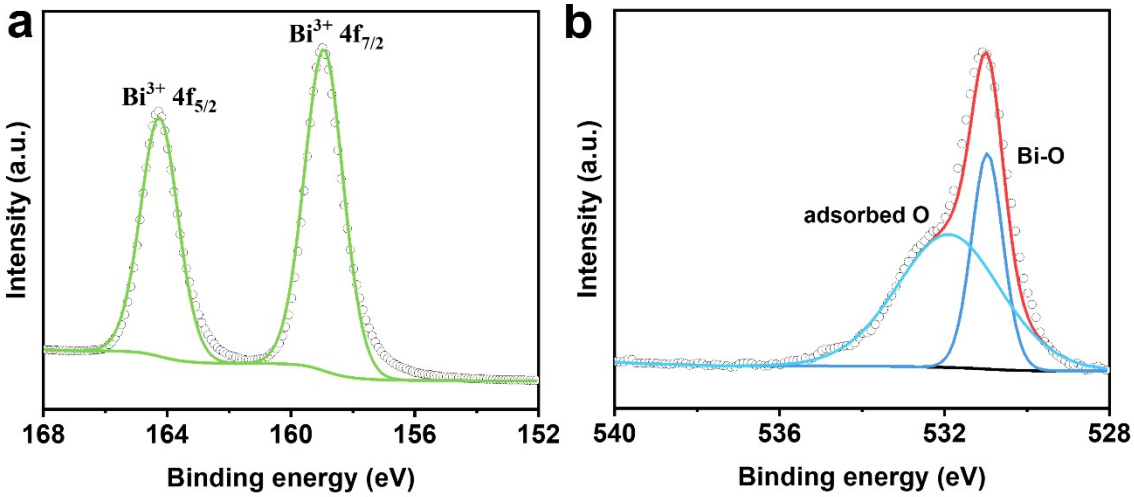

Figure S22. (a) Bi 4f and (b) O 1s XPS spectra of Bi_2O_3.

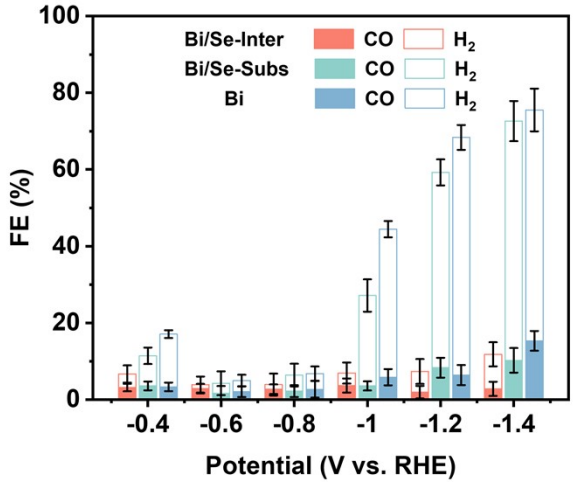

Figure S23. FE of H_2 and CO of Bi/Se-Inter, Bi/Se-Subs and Bi under different potentials.

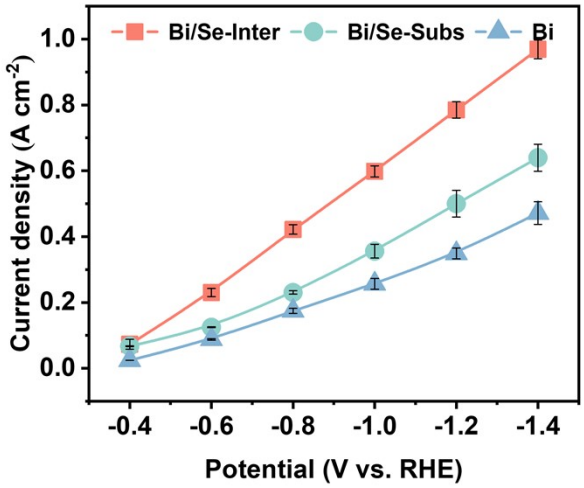

Figure S24. Total current density of Bi/Se-Inter, Bi/Se-Subs and Bi under different potentials.

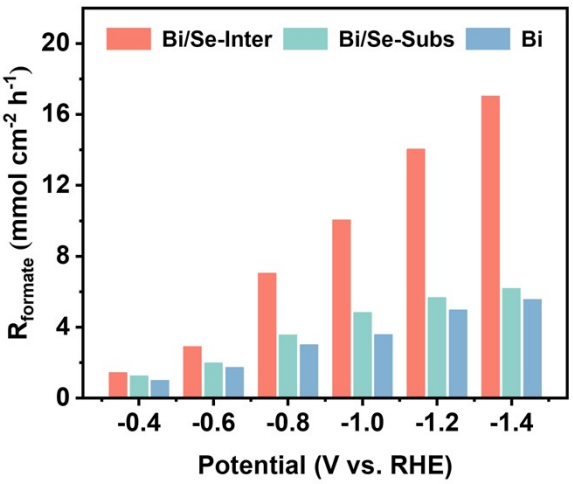

Figure S25. $R_{formate}$ of Bi/Se-Inter, Bi/Se-Subs and Bi under different potentials.

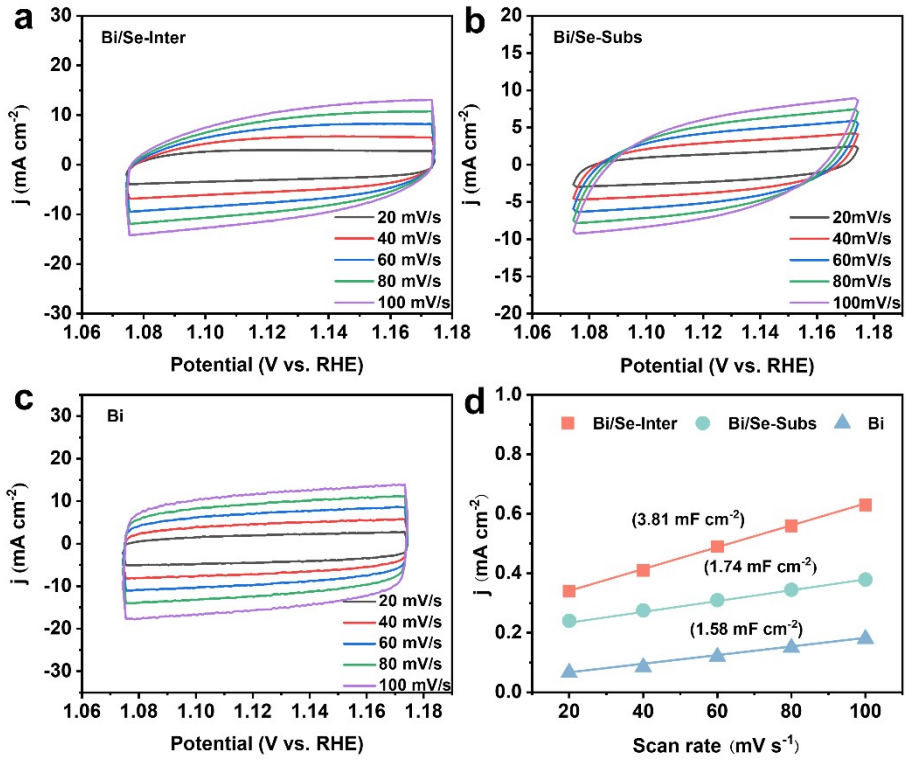

Figure S26. Electrochemically active surface area measurement. CV curves of (a) Bi/Se-Inter, (b) Bi/Se-Subs and (c) Bi. (d) Charging current density differences plotted against scan rates.

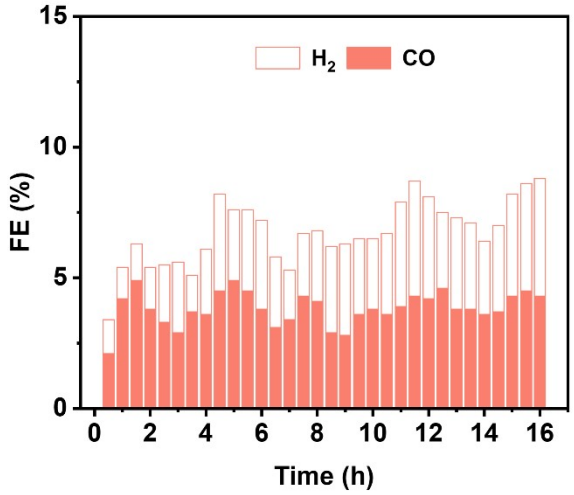

Figure S27. FE of H_2 and CO of Bi/Se-Inter over long-term stability.

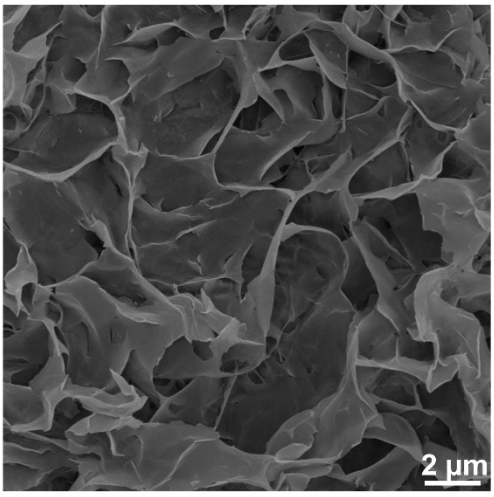

Figure S28. SEM image of Bi/Se-Inter after stability test.

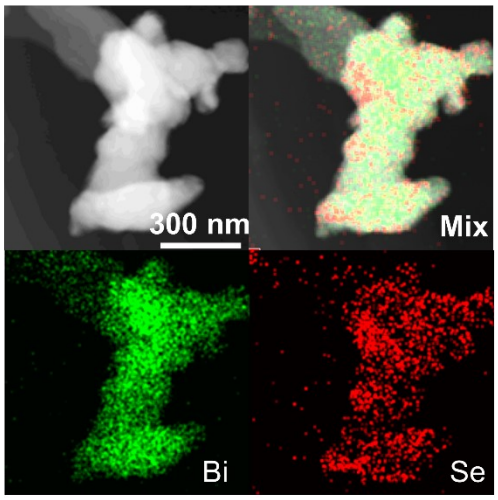

Figure S29. The EDS elemental mappings of Bi/Se-Inter after stability test.

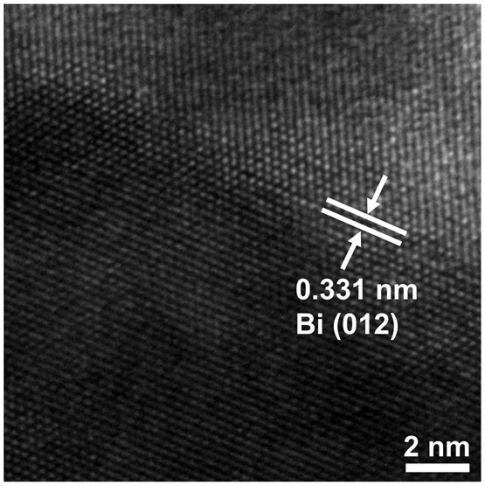

Figure S30. HRTEM image of Bi/Se-Inter after stability test.

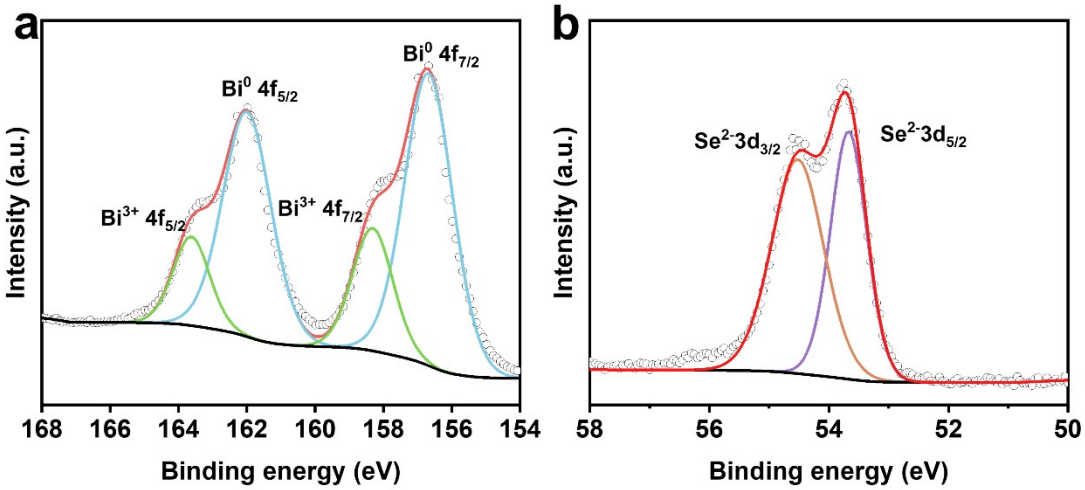

Figure S31. (a) Bi 4f and (b)Se 3d XPS spectra of Bi/Se-Inter after stability test.

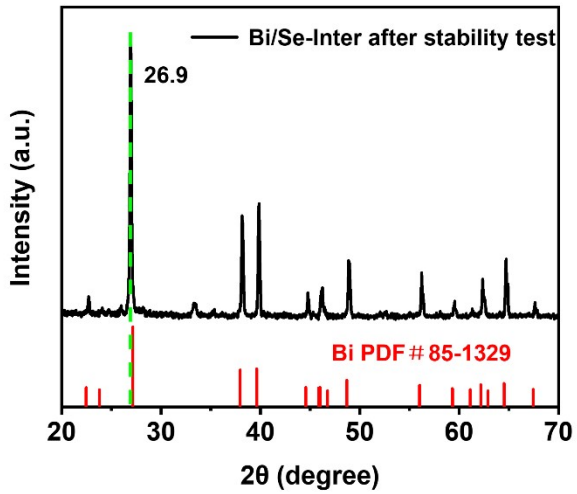

Figure S32. XRD pattern of Bi/Se-Inter after stability test.

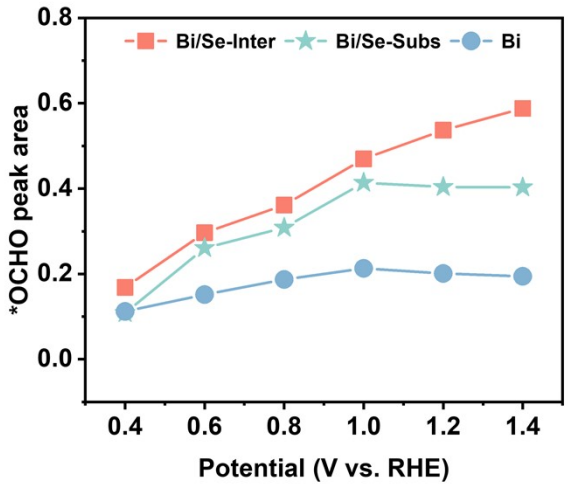

Figure S33. Relative intensity of the *OCHO intermediate on Bi/Se-Inter, Bi/Se-Subs and Bi at the different potentials.

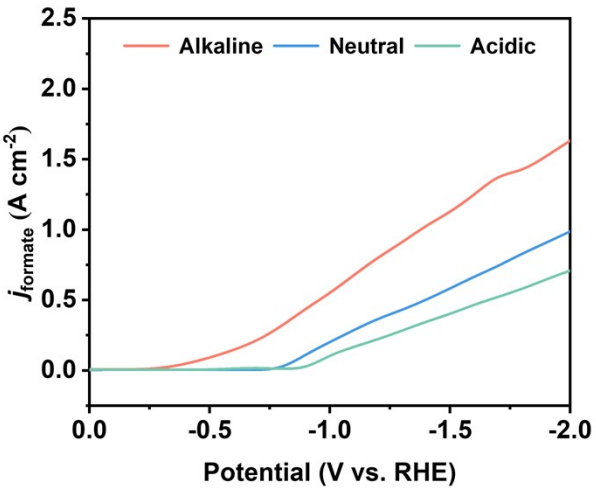

Figure S34. LSV curves of Bi/Se-Inter in alkaline (1 M KOH), neutral (0.5 M K_2SO_4) and acidic (0.05 M H_2SO_4 + 0.5 M K_2SO_4) electrolyte.

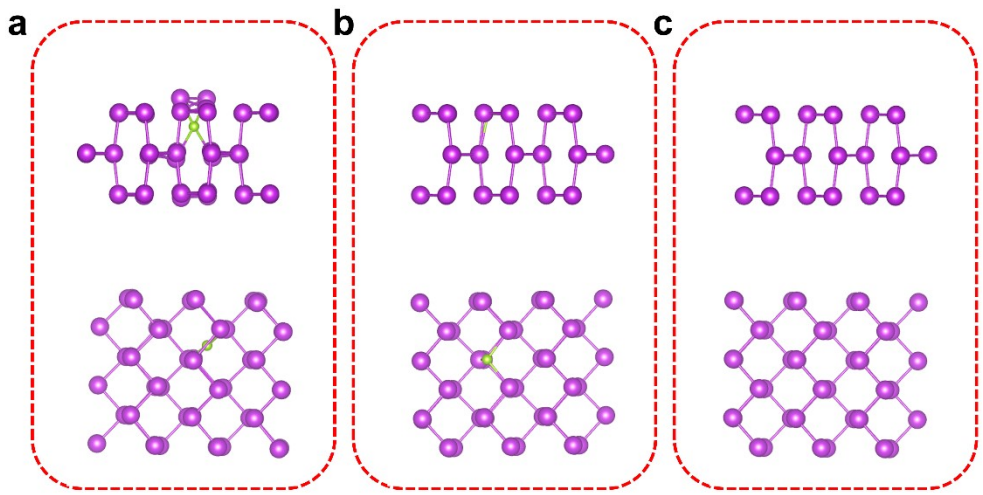

Figure S35. Side view and top views for the three models: (a) Bi/Se-Inter, (b) Bi/Se-Subs, and (c) Bi in DFT calculations. Color code: purple for Bi, green for Se.

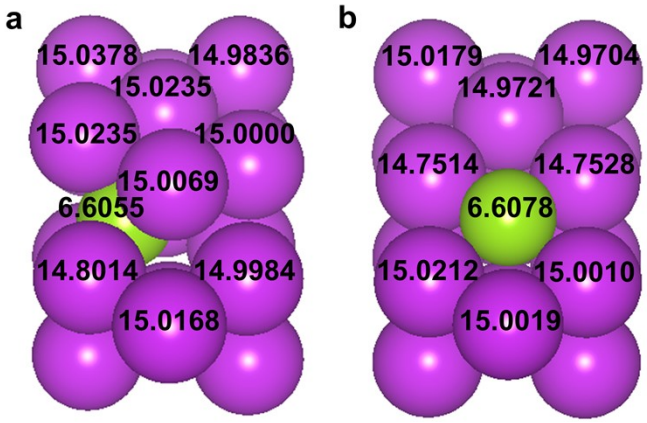

Figure S36. Bader charge calculation of Bi/Se-Inter (a) and Bi/Se-Subs (b). Color code: purple for Bi, green for Se.

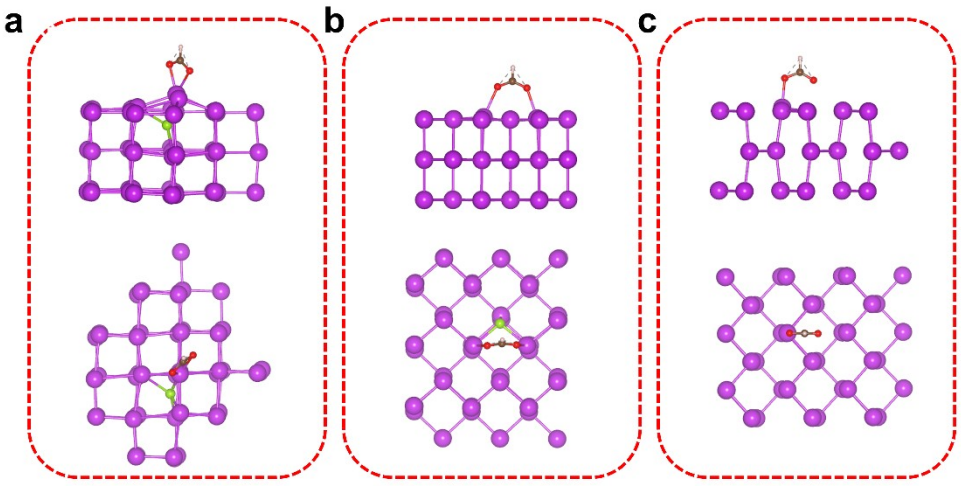

Figure S37. Side view and top views for the three models with *OCHO adsorbate: (a) Bi/Se-Inter, (b) Bi/Se-Subs, and (c) Bi. Color code: purple for Bi, green for Se, red for O, brownness for C, pink for H.

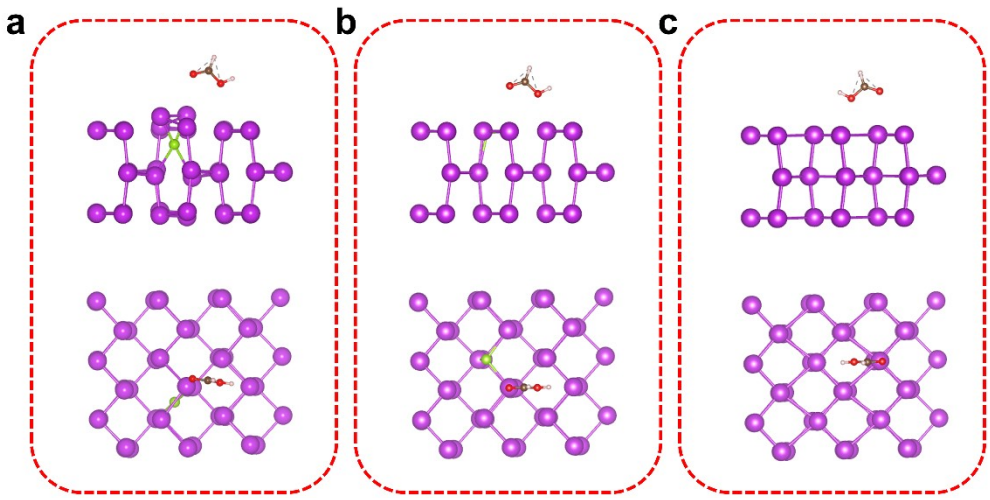

Figure S38. Side view and top views for the three models with *HCOOH adsorbate: (a) Bi/Se-Inter, (b) Bi/Se-Subs, and (c) Bi. Color code: purple for Bi, green for Se, red for O, brownness for C, pink for H.

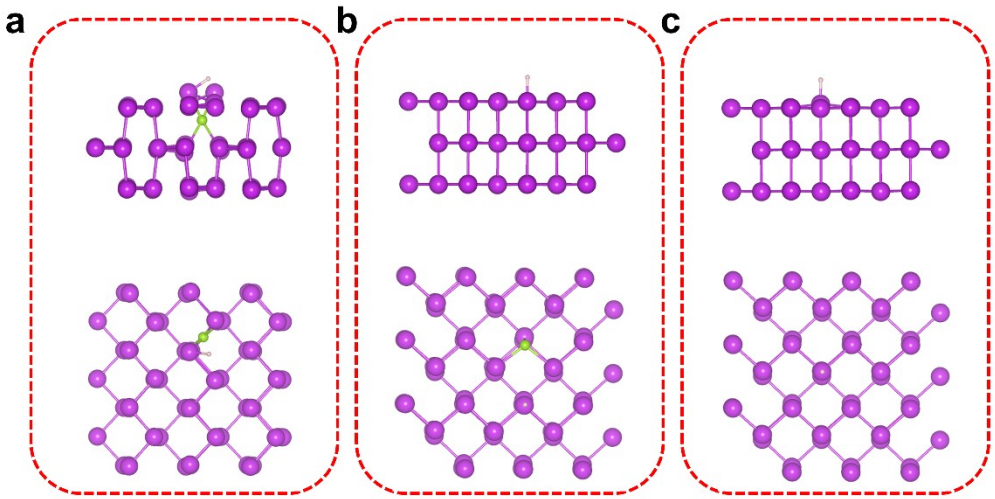

Figure S39. Side view and top views for the three models with *H adsorbate: (a) Bi/Se-Inter, (b) Bi/Se-Subs, and (c) Bi. Color code: purple for Bi, green for Se, pink for H.

Table S1. The comparison of the formate products performance reported in recent literature.

Catalyst	Electrolyte	$FE_{formate}$ (%)	$J_{formate}$ (mA cm^{-2})	Reference
Bi/Se-Inter	1M KOH	98.1	413	This work
		95.7	572	
		96.7	759	
		91.4	885	
VS-Bi_2O_3	1 M KOH	93.7	400	[1]
InNCN	1 M $KHCO_3$	81.4	407	[2]
PD-Bi	1 M KOH	90.2	450	[3]
nBuLi-Bi	2 M KOH	82	500	[4]
Bi-ene-NW	1 M KOH	91	570	[5]
Sn2.7Cu	1 M KOH	85.3	590	[6]
O-Bi-ene	2 M KOH	87.5	675	[7]
InP	1 M KOH	82.8	712	[8]
RLD Bi NSs	1 M KOH	91	800	[9]
BS/VC	1 M KOH	85.9	800	[10]
500-In_2O_3	1 M KOH	97.1	510	[11]

Table S2. The FE of Bi/Se-Inter at different times and for different products in the long-term stability test.

Time	$FE_{formate}$ (%)	FE_{CO} (%)	FE_{H2} (%)
0.5	94.0	2.0	4.0
1.0	94.5	1.7	3.8
1.5	95.0	1.5	3.5
2.0	94.8	1.5	3.7
2.5	95.2	1.2	3.6
3.0	94.6	1.5	3.9
3.5	95.0	2.2	3.8
4.0	94.9	1.4	3.7
4.5	95.1	1.3	3.6
5.0	94.7	1.4	3.9
5.5	95.0	1.2	3.8
6.0	94.8	1.5	3.7
6.5	95.2	2.2	3.6
7.0	94.6	1.5	3.9
7.5	95.1	1.2	3.8
8.0	94.7	1.4	3.7
8.5	95.0	2.5	3.6
9.0	94.8	2.2	3.9
9.5	95.2	1.4	3.8
10.0	94.6	3.3	3.7
10.5	94.3	2.5	3.6
11.0	95.0	1.4	3.9
11.5	94.9	2.2	3.8
12.0	95.1	3.1	3.7
12.5	94.7	2.4	3.6
13.0	95.0	1.9	3.9
13.5	94.8	1.4	3.8
14.0	95.2	2.6	3.7
14.5	94.6	2.4	3.6
15.0	95.0	2.8	3.1
15.5	94.9	2.9	3.9
16.0	95.1	2.1	2.8

Table S3. The FE of Bi at different times and for different products in the long-term stability test.

Time	$FE_{formate}$ (%)	FE_{CO} (%)	FE_{H2} (%)
0.5	92.6	2.1	5.3
1.0	94.2	1.8	4.0
1.5	93.8	1.7	4.5
2.0	91.56	2.0	6.5
2.5	90.3	1.9	7.8
3.0	91.6	2.2	10.2
3.5	90.1	2.0	8.9
4.0	91.7	2.3	13.0
4.5	89.9	2.1	7.0
5.0	85.4	2.4	18.2
5.5	81.6	2.2	16.2
6.0	76.8	2.3	20.9
6.5	72.1	2.5	25.5

Table S4. Adsorption energy of *OCHO on the Bi/Se-Inter, Bi/Se-Subs and Bi models.

Models	E (eV)
Bi/Se-Inter	-2.513
Bi/Se-Subs	-2.481
Bi	-2.285

References

[1] Y. Shi, C. F. Wen, X. Wu, J. Y. Zhao, F. Mao, P. F. Liu, H. G. Yang, Materials Chemistry Frontiers 2022, 6, 1091-1097.

[2] B. Jia, Z. Chen, C. Li, Z. Li, X. Zhou, T. Wang, W. Yang, L. Sun, B. Zhang, J. Am. Chem. Soc. 2023, 145, 14101-14111.

[3] Y. Xing, H. Chen, Y. Liu, Y. Sheng, J. Zeng, Z. Geng, J. Bao, Chem. Commun. 2021, 57, 1502-1505.

[4] L. Fan, C. Xia, P. Zhu, Y. Lu, H. Wang, Nat. Commun. 2020, 11, 3633.

[5] M. Zhang, W. Wei, S. Zhou, D.-D. Ma, A. Cao, X.-T. Wu, Q.-L. Zhu, Energ. Environ. Sci. 2021, 14, 4998-5008.

[6] K. Ye, Z. Zhou, J. Shao, L. Lin, D. Gao, N. Ta, R. Si, G. Wang, X. Bao, Angew. Chem. Int. Edit. 2020, 59, 4814-4821.

[7] B. Ning, Q. Xu, M. Liu, H. Jiang, Y. Hu, C. Li, Chem. Eng. Sci. 2022, 251, 117409.

[8] B. Zhang, Y. Chang, P. Zhai, C. Wang, J. Gao, L. Sun, J. Hou, Adv. Mater. 2023, 35, 2304379.

[9] Z. Wang, X. Zu, X. Li, L. Li, Y. Wu, S. Wang, P. Ling, Y. Zhao, Y. Sun, Y. Xie, Nano Research 2022, 15, 6999-7007.

[10] J. Zhu, J. Li, R. Lu, R. Yu, S. Zhao, C. Li, L. Lv, L. Xia, X. Chen, W. Cai, J. Meng, W. Zhang, X. Pan, X. Hong, Y. Dai, Y. Mao, J. Li, L. Zhou, G. He, Q. Pang, Y. Zhao, C. Xia, Z. Wang, L. Dai, L. Mai, Nat. Commun. 2023, 14, 4670.

[11] Z. Zhu, Y. Zhao, P. Sun, Y. Sun, X. Ma, Y. Dong, Z. Zhang, A. N. Alodhayb, X. Yi, W. Shi, Z. Chen, J. Energy. Chem. 2025, 105, 54-64.